Peripheral Binding Mode and Penetration Depth of Cobra Cardiotoxin on Phospholipid Membranes as Studied by a Combined FTIR and Computer Simulation Approach†

Wei-Ning Huang, Shih-Che Sue, Da-Shin Wang, Po-Long Wu, and Wen-guey Wu*

Institute of Bioinformatics and Structural Biology, National Tsing Hua University, Hsinchu, 30043, Taiwan

Received March 18, 2003; Revised Manuscript Received May 6, 2003

ABSTRACT: Cobra cardiotoxin, a cytotoxic β-sheet basic polypeptide, is known to cause membrane leakage in many cells including human erythrocytes. Herein, we demonstrate that the major cobra cardiotoxin from *Naja atra*, CTX A3, can cause leakage of vesicle contents in phosphatidylglycerol (PG) and phosphatidylserine containing, but not in pure phosphatidylcholine (PC), membrane bilayers. By the combined polarized attenuated total reflection infrared spectroscopy and computer simulation studies, CTX A3 is shown to peripherally bind to both zwitterionic and anionic monolayers in a similar edgewise manner with a tilted angle of $\sim 48 \pm 20°$ between the β-sheet plane of the CTX molecule and the normal of the membrane surface. The average surface area expansion induced by CTX A3 binding to the PG monolayer, however, is two times larger than that of the PC monolayer as determined by the Langmuir minitrough method. Interaction energy considerations of CTX A3 on neutral and negatively charged membrane surfaces suggests that the electrostatic interaction between anionic lipid and cationic CTXs plays a role in modulating the penetration depth of CTX molecules on the initial peripheral binding mode and reveals a pathway leading to the formation of an inserted mode in negatively charged membrane bilayers.

Cobra cardiotoxins (CTXs)[1] are amphiphilic, all β-sheet, basic polypeptides of 60−62 amino acid residues with a three-fingered loop folding topology. In vivo, CTXs cause systolic heart arrest, severe tissue necrosis, and/or blindness of the eye (*1*). In vitro, general cytotoxicity toward many cell types such as human erythrocytes, cancer cells, and cardiomyocytes has been demonstrated (*2*−*4*). Depending on the experimental conditions, CTXs have also been shown to induce aggregation, fusion, and membrane leakage of phospholipid vesicles (*5*−*7*). The study on the structure and activity relationship of the interaction of CTXs with membrane phospholipids reveals an important role of hydrophobic amino acid residues located at the tips of the three-fingered loop to promote CTX−lipid interaction (*8*−*10*). The 3-D structures of various CTX homologues in both aqueous and micellar environments (*9*−*11*) are available, and CTX molecules are unlikely to adopt large conformational changes because of the presence of four disulfide bonds. CTXs may, therefore, serve as a good model system for the study of protein−lipid interaction in understanding the mechanism responsible for the general cytolytic action of many amphiphilic antimicrobial polypeptides.

Recent advances in both experimental and theoretical studies of the interaction of antimicrobial and fusion peptides with lipid bilayers have indicated many physical rearrangement steps of the studied molecules within the membrane environment (*12*, *13*). For instance, a binding-induced conformational change (*14*), reorientation of the protein from a peripheral binding to an insertion mode (*15*), and oligomerization of the inserted proteins (*16*) are needed if these molecules are to be considered to form transmembrane pores. Under favorable conditions, various spectroscopic investigations of CTXs with model membrane systems have indeed shown an enhanced β-sheet formation of CTX molecules (*17*) and the existence of oligomeric states (*7*). More than one orientation of CTX molecules near the membrane surface has been reported (*18*). More interestingly, anionic lipids have been detected to play a structural role in the formation of CTX dimers (*7*). What remains to be established is to determine the initial peripheral binding mode and to understand the mechanism responsible for the CTX translocation to an inserted mode.

Previous characterization by infrared spectroscopy of the interaction of CTX with phosphatidic acid films (*19*) indicates that the orientation of CTXs with respect to the

† This work was supported by National Science Council NSC-91-2113-M-007-041 and MOE Program for Promoting Academic Excellence of Universities under Grant 89-B-FA04-1-4.

* Corresponding author. Tel: 886-3-573-1040. Fax: 886-3-571-5934. E-mail: wgwu@life.nthu.edu.tw.

[1] Abbreviations: ATR, attenuated total reflection; 6-CF, 6-carboxyfluorescein; CTX, cardiotoxin; DMPC, 1,2-dimyristoyl-*sn*-glycero-3-phosphocholine; DMPG, 1,2-dimyristoyl-*sn*-glycero-3-phosphoglycerol; FTIR, Fourier transformed infrared spectroscopy; HPLC, high performance liquid chromatography; LPC, 1-myristoyl-2-hydroxy-*sn*-glycero-3-phosphocholine; LUVs, large unilamellar vesicles; POPG, 1-palmitoyl-2-oleoyl-*sn*-glycero-3-phosphoglycerol; POPS, 1-palmitoyl-2-oleoyl-*sn*-glycero-3-phosphoserine; POPC, 1-palmitoyl-2-oleoyl-*sn*-glycero-3-phosphocholine.

10.1021/bi0344477 CCC: $25.00
Published on Web 05/30/2003

bilayer surface is not homogeneous. Recent solid-state NMR studies of CTX with dipalmitoyl PC bilayers suggest that CTX orientation is sensitive to the lateral packing density and hydrophobic thickness of the lipid membrane (*20*). However, high-resolution NMR studies on the CTX/micellar complex indicate a predominant peripheral binding mode of CTX in PC micelles involving the three-fingered hydrophobic tips of the P-type CTXs (*9*, *10*). These results suggest a dynamic feature of CTX−phospholipid interaction. It is therefore important to develop experimental systems that can trap each step of the interaction dynamics so that the cytolytic action of CTXs can be understood.

In an effort to determine and compare the peripheral binding mode of CTXs toward neutral and anionic phospholipid membranes, we first developed a monolayer system that prevented the formation of an inserted binding mode. Specifically, we performed polarized attenuated total reflection (ATR) infrared spectroscopy to study the binding of CTX A3 molecules, the major P-type CTX from Taiwan cobra venom, with phospholipid monolayers, which are then transferred on an ATR germanium crystal to be measured by ATR−IR spectroscopy. A well-defined orientation of CTX A3 with respect to both neutral and anionic monolayers transferred on a germanium crystal can be identified. The results not only demonstrate the feasibility of combining ATR−IR spectroscopy with mean field energy analysis to determine the binding mode of amphiphilic polypeptides on the membrane surface but also to emphasize the role of electrostatic interaction to modulate (or regulate) the hydrophobic interaction between the amphiphilic polypeptides and the phospholipid membrane.

MATERIALS AND METHODS

Crude venom from *Naja atra* was purchased from Sigma Chemical Company. CTX A3 was purified by SP-Sephadex C-25 ion exchange column chromatography followed by HPLC on a reverse-phase C-18 column as described previously (*5*). The 1,2-dimyristoyl-*sn*-glycero-3-phosphocholine (DMPC), 1,2-dimyristoyl-*sn*-glycero-3-phosphoglycerol (DMPG), 1-palmitoyl-2-oleoyl-*sn*-glycero-3-phosphoglycerol (POPG), 1-palmitoyl-2-oleoyl-*sn*-glycero-3-phosphoserine (POPS), 1-palmitoyl-2-oleoyl-*sn*-glycero-3-phosphocholine (POPC), and 1-myristoyl-2-hydroxy-*sn*-glycero-3-phosphocholine (LPC) used in this work were obtained commercially (Avanti Polar Lipids, Alabaster, AL). 6-Carboxyfluorescein (6-CF) was purchased from Sigma Chemical Co.

Vesicle Preparation. Lipids were dried under vacuum overnight and then hydrated with 10 mM Tris (pH 7.4), 75 mM NaCl, and 50 mM 6-CF. The suspension was frozen and thawed several times and was successively extruded through a polycarbonate filter with a pore size of 0.1 μm for obtaining homogeneous large unilamellar vesicles (LUVs). The Sepharose CL-4B column was used with 10 mM Tris buffer (pH 7.4) containing 150 mM NaCl to remove the residual fluorescent molecules outside of the vesicles, and the lipid concentration was determined by an inorganic phosphate assay as described (*21*).

Vesicle Leakage. Release of vesicle contents was detected by 6-CF fluorescence intensity. While 6-CF displays low fluorescence intensity at high concentration, its intensity increases sharply at low concentration. Vesicles containing 6-CF were incubated at a final volume of 1 mL of buffer in a 1 × 1 cm quartz cuvette. After addition of CTX, the fluorescence intensity was monitored as a function of time for the CTX induced vesicle leakage process. The 6-CF leakage was calculated using the following expression: leakage % = $(F_t - F_i)/(F_f - F_i)$, where F_i is the initial fluorescence before adding proteins, F_t is the fluorescence reading at time t, and F_f is the final fluorescence determined by adding 0.04% Triton (*18*). The excited and emitted wavelengths were 480 and 520 nm, respectively.

Monolayer. Monolayer experiments were done on a Langmuir minitrough (Joyce-Laebl Ltd.) with a home-built glass trough (16 × 11 × 2 cm, L × W × H) or 5 cm diameter Petridish for fixed surface pressure or area experiments, respectively. All trough outskirts used a Teflon belt to keep the lipid monolayer at a hydrophobic boundary. Data were collected by a personal computer directly connected to the experimental setup. The lipid was first dissolved in a chloroform/methanol 2:1 solution to a concentration of 1.5 mg/mL. It was then gently spread at the air−water interface in the trough with a microsyringe to form a lipid monolayer. For the fixed pressure experiment, the monolayer was then compressed to the setup pressure at a rate lower than 5 Å^2 molecule^{-1} min^{-1} (*22*). The surface pressure was measured by the Wilhelmy plate method using plates cut from filter paper (Whatman No. 1). The subphase solution was 100 mM NaCl and 1 mM phosphate buffer (pH 7.4). The temperature was maintained at 25 °C.

Measurement of the Penetration Area. Three different methods were applied to estimate the penetration area of CTX A3 near the membrane surface. The first method is the direct determination of the CTX concentration on the monolayer surface by using FTIR spectroscopic techniques, and the penetration area is simply estimated by the ratio of the surface area expansion as determined by the monolayer method and the total amount of CTX molecules bound to the membrane surface as determined by FTIR. The second method is to estimate the cross-section area of the CTX molecule according to the 3-D structure of CTX A3/LPC micelles generated by NMR intermolecular NOE experiments and that of the CTX A3/SDS complex as determined by X-ray diffraction at 1.9 Å resolution (*17*). The third method is the free energy method by measuring the variation of the partition coefficient, K_{app}, with the lateral surface pressure, π. It has previously been shown that

$$K_{app} = K_o \exp(-\pi A_p/kT) \quad (1)$$

where K_o is the proportionality constant and A_p is the cross-sectional area of the peptide portion in the lipid monolayer. If the assumption of constant area can be made for less than a 15% change in the given surface pressure interval, $\Delta A/A$, as a result of CTX binding, it can be shown that

$$K_{app} \propto \Delta A/A = \text{const.} \exp(-\pi A_p/kT) \quad (2)$$

According to eq 2, the penetration area, A_p, is determined from the slope of ln $\Delta A/A$ versus the π curve (*23*).

Fourier Transformed Infrared Spectroscopy (FTIR). FTIR spectra were recorded on a Boman DA8.3 spectrometer equipped with a CaF_2 beam splitter and a liquid nitrogen-

cooled MCT detector. The spectra (1000 scans) were recorded at a spectral resolution of 2 cm^{-1} with triangular apodization, and the incoming radiation was polarized with a germanium single diamond polarizer (Harrick, Ossining, NY). The 45° germanium ATR-plate (2 × 5 × 50 mm) was cleaned by plasma cleaner (Harrick, Ossining, NY) before the samples of lipid−protein monolayer were read. The transfer rate was kept at 0.5 cm/min^{-1}.

To obtain the standard calibration curve of the protein/lipid ratio of the monolayer, a different molar ratio lipid/CTX was dissolved in a chloroform/methanol solution (2:1) and air-dried on an ATR germanium crystal (*24*). Regular spectra rather than polarized IR spectra were performed for these standard curves, and it was reduced to 300 scans. We compare the IR intensity of the lipid ester bond and protein amide I range of nonpolarized standard spectra with monolayer $A_{\parallel} - 0.42A_{\perp}$ to determine the ratio of CTX and lipid (*25*).

Dichroic Ratio Map. The vibrational moments of amide I and II in polypeptides are known to be perpendicular to and parallel with the β-sheet plane, respectively (*26*, *27*). Therefore, it is possible to apply directly the 3-D coordinates of the CTX A3 structure for summing up the amide I or II vibrational moment of each residue under a different rotation angle of (θ, ϕ) to generate a theoretical map for the dichroic ratio of CTX A3. It should be emphasized that the 3-D structure of CTX A3 remains mostly the same, except for those residues near the tip of the loop, in the presence and absence of LPC or SDS micelles. Therefore, the dichroic ratio map can be generated faithfully for CTX A3 without having to worry about the lipid-induced conformational change of the studied molecule.

In brief, ATR interface electric field amplitudes (28) are given by

$$E_x = \frac{2\cos\gamma\sqrt{\sin^2\gamma - n_{31}^2}}{\sqrt{1-n_{31}^2}.\sqrt{(1+n_{31}^2)\sin^2\gamma - n_{31}^2}}$$

$$E_y = \frac{2\cos\gamma}{\sqrt{2-n_{31}^2}}$$

$$E_z = \frac{2\cos\gamma n_{32}^2\sin\gamma}{\sqrt{1-n_{31}^2}.\sqrt{(1+n_{31}^2)\sin^2\gamma - n_{31}^2}} \quad (3)$$

where E_x, E_y, and E_z represent the electric field amplitudes along the x, y, and z axes; n_1, n_2, and n_3 are the refractive indices of germanium, a thin film on germanium surface, and the air, respectively; $n_{31} = n_3/n_1$ and $n_{32} = n_3/n_2$; and γ is the angle of incidence between beam and normal to the crystal surface. The infrared linear dichroic ratio is defined by

$$R_z = A_{\parallel}/A_{\perp} = \frac{\langle M_x^2\rangle E_x^2 + \langle M_z^2\rangle E_z^2}{\langle M_y^2\rangle E_y^2} \quad (4)$$

where $A_{\parallel}$ and $A_{\perp}$ are the absorbances for radiation polarized parallel and perpendicular, respectively, and $\langle M_x^2\rangle$, $\langle M_y^2\rangle$, and $\langle M_z^2\rangle$ are the total transition moment square of CTX at three different axes. For a random distribution of molecular orientation in the xy plane, integration must be performed over this plane, and the resulting dichroic ratio is given by

$$R_z = \frac{E_x^2}{E_y^2} + \frac{\langle M_z^2\rangle E_z^2}{[(\langle M_y^2\rangle + \langle M_x^2\rangle)/2]E_y^2} \quad (5)$$

The dichroic ratio maps of amide I and II can then be calculated according to eqs 4 and 5 with parameters of $n_1 = 4$, $n_2 = 1.43$, $n_3 = 1$, and $\gamma = 45°$. The maps have φ angle symmetry because the values of the dichroic ratio are the same where the protein faces the z axis or membrane.

Interaction Energy Map. A mean field approach, or the so-called implicit solvent method, is used for the computer simulation studies to obtain the interaction energy of the CTX A3 molecule at the membrane surface. Normally, the interaction energy consists of two parts: (i) the internal energy of the residue that depends on the conformation of the peptide and (ii) surrounding terms that depend on the position of the amino acid. The internal energy is involved in the conformational changes of the peptide between the bulk and the membrane phases. Since our calculations focus on the determination of the interaction energy for CTX A3 under different orientations at the membrane surface, one assumed that the difference of internal energy is insignificant and could be neglected (*29*). The energy calculation could then be reduced to a surrounding term with the combined (i) hydrophobic energy, E_{hydro}, of amino acid residues in the membrane environment and (ii) electrostatic energy, E_{elect}, of protein charge interaction with the membrane lipid headgroup potential according to the following equation:

$$E_{total} = E_{hydro} + E_{elect} \quad (6)$$

The hydrophobic energy of a residue is a function of the z-coordinated y $f(z_i)$. Thus, the CTX/monolayer interaction energy is given by

$$E_{hydro} = \sum_i H_i f(z_i) \quad (7)$$

where summation is over the residues, and $z_i = 0$ corresponds to the interface of the monolayer and bulk phase. A hydrophobicity index, H_i (*30*, *31*), is applied to the C_α atom of each amino acid residue, and the C- and N-terminal hydrophobicity index is applied to the nitrogen and carbon atom, respectively. Each hydrophobic value of the residue was determined by the free energy of transport of the amino acid from the interface to the interior of a bilayer, and the values of the transport free energy were smaller than nonstructure amino acids' values (*32*). To obtain a continual and smooth energy value, the $f(z_i)$ function is given by (*31*)

$$f(z_i) = 0.5\exp(-z_i/\lambda) \text{ where } z_i > 0$$

$$f(z_i) = 1 - 0.5\exp(z_i/\lambda) \text{ where } z_i < 0 \quad (8)$$

Thus, for a residue i the hydrophobic energy is H_i within the monolayer, and it is zero outside the monolayer. The value of λ defines the transition from the bulk phase to the monolayer phase and is 1 Å.

The electrostatic term representing the effects of the membrane headgroup potential is given by

$$E_{elect} = \sum_i q_i \Phi(z_i) \quad (9)$$

where q_i and $\Phi(z_i)$ are the residue charge and membrane headgroup potential profile along the monolayer normal, respectively. In this study, we use molecular dynamic simulation results of zwitterionic and anionic phospholipid bilayers as our membrane headgroup potential (Figure 5A) (*33*, *34*). It should be pointed out that the electrostatic potential profile of molecular dynamic simulation is different from that generated by the method of combining asymmetry dielectric constants and charge density (*35*).

The CTX A3 molecule (PDB 1I02) was initially laid at the interface (*xy* plane), and the centered β-strand was aligned along the *y* axis. The notation of (θ, φ) for the interaction energy map is the same as that for the dichroic ratio map. It is possible to estimate the population of a different CTX A3 orientation according to the Boltzmann distribution:

$$I_{state}/(I_{state} + S_{state}) = \exp(-(E_i - E_s)/kT) \quad (10)$$

where E_i, E_s, k, and T are energy at the designated state of i and s, Boltzmann constant, and temperature, respectively. All calculation programs were written in QuickBasic 4.5 and run on a personal computer. The program is available upon request.

NMR Spectroscopy and Intermolecular NOE Measurement. The NMR samples of the CTX/LPC and CTX/D-LPC complexes were prepared by dissolving a desired amount of CTX A3 and lipid into 500 μL of a 90% H_2O/10% D_2O mixture with 10 mM phosphate buffer to reach a final molar ratio of 1:50 (1:50 mM). The samples were used to determine intermolecular NOEs by 2-D NOESY experiments. The pH of the sample was adjusted to 6.0 $\pm$ 0.1 by titrating with NaOH and HCl.

2-D NOESY experiments with a 150 ms mixing time were recorded on a Bruker DRX600 spectrometer equipped with a 5 mm triple resonance probe (*36*). Water suppression was achieved by a pulsed field gradient with the 3-9-19 WATERGATE sequence. All NMR experiments were performed at 45 °C to overcome the problem of NMR line width broadening. The 2-D spectra were typically acquired with 2048 complex data points in the t_2 dimension and 512 points in the t_1 dimension with 192 scans per t_1 increment. Spectral processing was done by applying a $\sin^2$ window function in both dimensions followed by zero-filling to 2048 points in the t_1 dimension. The chemical shift was referenced to sodium 2,2-dimethyl-2-silapentane-5-sulfonate (DSS) at 0.015 ppm. Data processing was done on a Silicon Graphics O2 workstation using the XWINNMR program.

The identification of CTX A3 and LPC proton chemical shifts were based on the data obtained by 2-D NOESY experiments and previous chemical shift assignments (*11*). Two 1-D slices of bulk methylenes, $(CH_2)_{12}$, of fatty acyl chains and choline methyls, $N^+(CH_3)_3$, of the headgroup were extracted from the resonance of 1.28 and 3.23 ppm at the ω1 dimension to help identify the intermolecular NOEs between protein and lipid tail and head regions. A spectrum obtained with a complex of CTX A3 with deuterated LPC was used to further confirm the assignments of intermolecular NOEs between the protein and the lipid tail region by comparing the refereed 1-D slice.

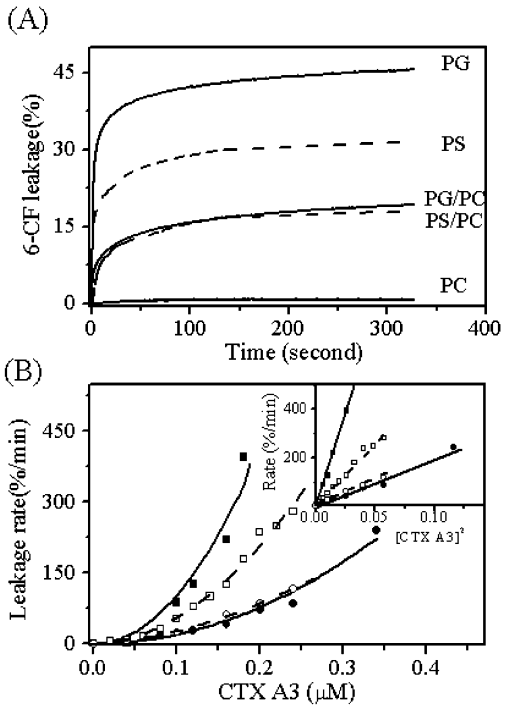

FIGURE 1: (A) CTX A3-induced leakage of 6-CF of phospholipid vesicles with indicated lipid composition. Concentrations of CTX and vesicle were 0.16 and 10 μM, respectively. (B) Initial rate of 6-CF leakage as a function of CTX A3 concentration, pure POPG (■); 50% POPG/POPC (●); pure POPS (□); and 50% POPS/POPC (○). Inset replots the data shown in panel B with the square of toxin concentration.

RESULTS AND DISCUSSION

CTX A3 Induces Vesicle Leakage in the Anionic Membrane. Shown in Figure 1A are the representative traces of time-dependent CTX A3-induced leakage of a 6-CF fluorescence probe trapped in large unilamellar vesicles (LUVs with a diameter of ~1000 Å) with the indicated lipid composition. Although there is no detectable leakage of PC vesicles, the introduction of negatively charge lipids such as POPG or POPS produces significant effects. While the extent CTX-induced leakage of the pure POPG vesicle is almost 50% larger than that of the POPS vesicles, the effects on the 50% POPG/POPC and POPS/POPC vesicles are about the same. A concentration dependent study of such an effect further indicates that the initial leakage rates increase as a square of the CTX A3 concentration for all the phospholipids used for this study (Figure 1B). It suggests that a bimolecular interaction of CTX A3 might be a rate-limiting step responsible for the leakage process. Since the effects are similar for the two lipid samples with different headgroup structure of the POPG and POPS vesicles, the results further imply that electrostatic interactions between the anionic lipids and the cationic CTX A3 molecule play an important role.

Langmuir Monolayer Experiment. Shown in the inserted panel of Figure 2A is the representative binding traces of CTX A3 toward the DMPC monolayer as reflected by a pressure increase (ΔmN/m) upon treatment with 50 nM CTX in 100 mM NaCl and 1 mM phosphate buffer at pH 7.4. The increase of monolayer pressure of the DMPC monolayer

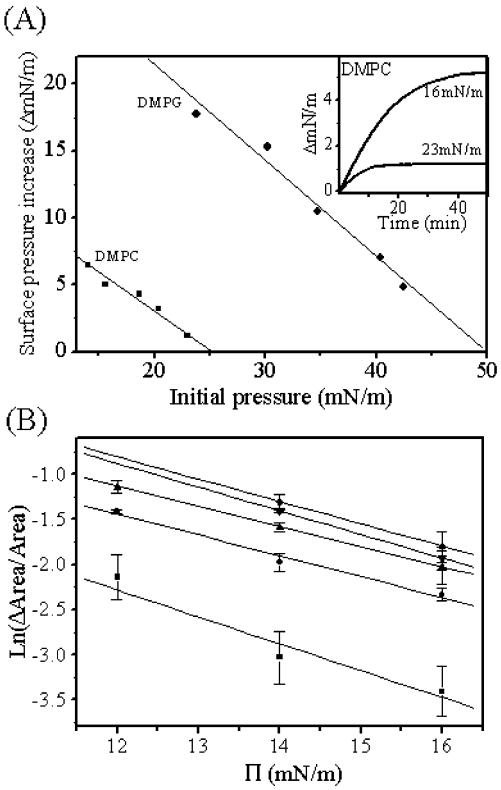

FIGURE 2: (A) Cobra cardiotoxin (CTX) binding-induced pressure increases as a function of initial pressure in zwitterionic DMPC and negatively charged DMPG monolayers. Insert plot shows two representative traces of the surface pressure change as a function of time upon addition of CTX (50 nM) into the DMPC monolayer at an initial surface pressure of 16 and 23 mN/m. The pressure increase is determined as the increment in maximum value of surface pressure when the traces reach plateau. (B) Relative surface area expansion, ln(ΔA/A), of DMPC monolayers as a function of the surface pressure at various CTX concentrations: 10 nM (■); 30 nM (●); 50 nM (▲); 70 nM (▼); and 90 nM (◆).

is found to be 1 and 5 ΔmN/m for the initial monolayer pressure of 23 and 16 mN/m, respectively. Similar binding curves, but with a much larger effect, can also be observed for the anionic DMPG monolayer (data not shown). The respective cutting-off pressure for a detectable CTX A3 binding of the DMPC and DMPG monolayers as extrapolated from the initial pressure dependent studies is found to be 25 and 50 mN/m (Figure 2). These results are consistent with the previous observation that the CTX molecule can penetrate into the monolayer of anionic lipids at an equivalent bilayer pressure of 30 mN/m but interact with the monolayer of the zwitterionic lipid only at a much lower pressure condition (*37*). In fact, significant binding of CTX toward zwitterionic PC or sphingomyelin membranes has only been reported for lipid micelles or for membrane bilayers near phase transition temperatures (*5*). The monolayer experiment suggests that the binding of CTX A3 to zwitterionic PC is simply too weak to attract enough CTX A3 to have significant surface area expansion.

Since a protein molecule has to perform the work $\Delta W = \pi A_p$, where A_p is the cross-section of protein, to penetrate into a lipid monolayer with a lateral pressure, π, it is possible to estimate the penetration area, A_p, based on the variation of the partition coefficient with the surface pressure π according to eq 2. By plotting $\ln(\Delta A/A)$ as a function of pressure π (Figure 2B), one can then obtain an estimated

Table 1: Values of the CTX Cross Section and Relative Penetration Depth Using Four Different Kinds of Measurement Methods

	Measurement methods			
	Gibbs energy (DMPC)	IR intensity (DMPC)	IR intensity (DMPG)	X-ray (SDS)
cross-section (Å^2)	104 ± 13	176 ± 24	370 ± 27	472 ± 19
penetration depth (Å)	3 ± 0.2	3.7 ± 0.3	6.8 ± 0.5	9.5 ± 0.5

penetration area A_p, or the cross-sectional area of the peptide in the DMPC monolayer, of 104 ± 13 Å^2 (Table 1). We could not determine the A_p in the DMPG monolayer by a similar pressure-dependent method since the liquid-expanded/liquid-condensed phase coexists when the surface pressure is higher than 32 mN/m (data not shown). The penetration area in the negatively charged membrane surface is then determined by direct measurements and geometrical methods in the following section.

FTIR Measurement. Polarized attenuated total reflection (ATR) infrared spectroscopic study of proteins (and polypeptides) in lipid bilayers has recently been established as a reliable method in determining the protein concentration and orientation with respect to membrane bilayers (*38*, *39*). To perform FTIR spectroscopic investigation on the orientation of CTXs near the membrane surface, germanium ATR-plates were then perpendicularly immersed into the lipid−water interface and slowly pulled out to allow the application of the desired phospholipid monolayer with a surface pressure of 14 and 30 mN/m for DMPC and DMPG, respectively. As we will demonstrate later, this method can indeed yield a well-defined orientation for CTX A3 on the membrane surface. The transfer ratio of the lipid/protein monolayer was found to be 1.00 ± 0.03, which indicated that the monolayer components pulling on the germaniun crystal is the same as the on air−bulk interface. We should point out that we did not perform the same kind of experiment on the PS membrane because the IR spectra of the lipid headgroup and protein amide region overlap with each other and are not suitable for quantitative analysis.

Quantitative analysis of the FTIR spectra on the signal intensity of the lipid (C═O vibration at 1739 cm^{-1}) and CTX (amide I vibration at 1648 cm^{-1}) provides a good correlation with the protein/lipid ratio as determined by chemical assay (Figure 3A). By knowing the amount of CTX molecules on the membrane surface from the FTIR signal intensity of lipid and CTX and the surface area expansion as measured by the Langmuir monolayer method, we can estimate the penetration area of the CTX A3 molecule on the DMPG and DMPC monolayer to be 370 ± 27 and 176 ± 24 Å^2 per CTX molecule, respectively (Table 1). We concluded that CTX A3 induces a larger surface area expansion in the anionic membrane than in the neutral membrane surface. It is, however, not clear whether the difference is due to the different binding mode in the two studied systems or simply because of their different penetration depths. It should also be noted that the penetration area determined by the direct spectroscopic method (i.e., 176 ± 24 Å^2 per CTX molecule) is significantly larger than the value determined by the pressure dependent (thermodynamic) method (i.e., 104 ± 13 Å^2 per CTX molecule). This is probably because of the assumption of the two binding states in deriving the equation

Table 2: Dichroic Ratio *R* for Selected Absorption Bands of Lipid and Lipid−CTX Monolayer Films Transferred on Ge Crystal[a]

	Frequency (cm^{-1})				
	2922 CH_2 antisym	2854 CH_2 sym	1739 C═O	1648 amide I	1525 amide II
DMPC	0.98 ± 0.04	0.99 ± 0.04	1.09 ± 0.05		
DMPG	0.98 ± 0.04	0.99 ± 0.04	1.11 ± 0.05		
DMPC + CTX	1.01 ± 0.04	0.98 ± 0.04	1.10 ± 0.05	1.26 ± 0.05	1.26 ± 0.06
DMPG + CTX	1.00 ± 0.04	0.99 ± 0.04	1.11 ± 0.05	1.25 ± 0.05	1.27 ± 0.06

[a] Langmuir tough surface pressure was fixed at 14 and 30 mN/m for DMPC and DMPG, respectively.

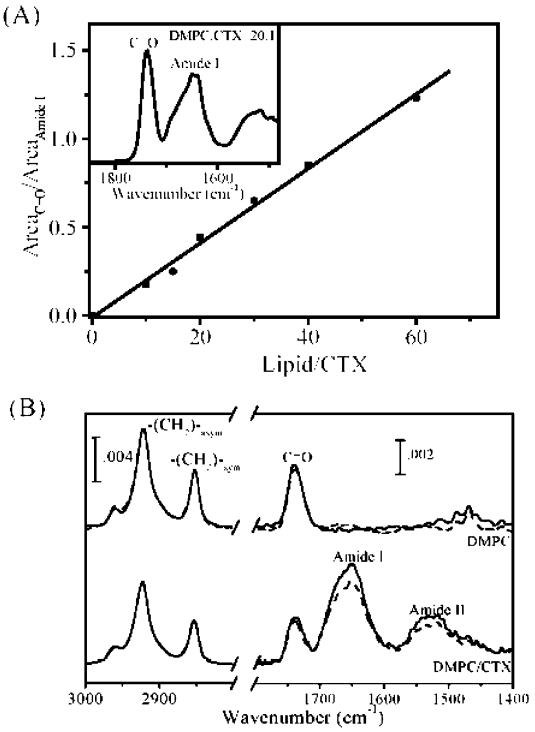

FIGURE 3: (A) Correlation of the FTIR signal intensity with lipid/protein ratio: DMPC (■) and DMPG (●). (B) Representative polarized ATR infrared spectra of DMPC monolayers transfer on a germanium crystal surface. Solid and dotted lines represent ATR IR spectra determined by parallel and perpendicular incident light, respectively. While the obtained polarized IR spectra for pure DMPC remain similar, a significant difference can be found for CTX (70 nM) molecules bound to DMPC monolayers 2 h after being added into the subphase. All the representative traces shown in the figure are measured at a surface pressure of 14 mN/m in 100 mM NaCl and 1 mM phosphate buffer at pH 7.4.

to estimate the penetration area according to the thermodynamic method.

The dichroic ratio *R* for selected absorption bands of the lipid and CTX are also experimentally determined and compared with the theoretical result (Figure 3B and Table 2). The *R* values of the CH_2 (at 2922 and 2854 cm^{-1}) and C═O (at 1739 cm^{-1}) vibrational modes of the phospholipid monolayers are found to be close to 1 and 1.1, respectively. Similar results have been reported for DPPC (*40*) and the PE-PG monolayer (*41*). Since there were no significant deviations of the *R* values determined for phospholipid when CTX bound on the membrane, it indicated that the lipid monolayer remains parallel to the germanium crystal upon CTX treatment. In contrast, the *R* value for the amide I and II vibrational mode of CTX A3 was found to be similar with a value of ~1.26 for both DMPC/CTX and DMPG/CTX samples. It suggests that CTX A3 not only has a well-defined orientation near the membrane surface but also adopts a similar orientation in either the neutral DMPC or the negatively charged DMPG monolayer. Since CTX is not homogeneously oriented in negatively charged membrane bilayers (*19*), the well-defined orientation of CTX A3 in the present monolayer system further implies that it probably needs two monolayer leaflets to provide a long hydrophobic thickness that is enough for the insertion of CTX molecules.

To compare the CTX binding modes in the neutral and anionic membrane surface using the FTIR method, we developed a new method of generating the dichroic ratio map for the determination of the orientation of the protein relative to the membrane surface. As we stated in the Materials and Methods, the dichroic ratio map for the different membrane orientation of CTX A3 can be theoretically estimated, provided that the 3-D structure of CTX A3 on the membrane surface is known. The vectors of the amide I and II vibrational moment of the protein are, respectively, 90 and 0° relative to the β-sheet structure strand. Therefore, one can generate a theoretical dichroic contour map of CTX A3 at various (θ, ϕ) angles (Figure 4A) for both the amide I (Figure 4B) and the amide II (Figure 4C) vibrational mode. These values are found to be in the range of 0.98−1.48 and 0.99−2.07 for amide I and II of the CTX A3 molecule, respectively. Lightly shaded areas in Figure 4, panels B and C are those values falling within the experimentally determined values of 1.26 ± 0.05. It can be seen that only two orientations of the CTX molecule with (θ, ϕ) angles highlighted by the dark shaded area are consistent with the experimental result. Consideration of the interaction energy between CTX and phospholipid membranes (Figure 5) further reveals that only the CTX orientation with (θ, ϕ) angles of (40°, 30°) is allowed for both neutral and negatively charged membranes. Consistent with previous NMR (*9*, *10*) and fluorescence spectroscopic investigations (*18*) of P-type CTX with phospholipid micelles, the determined orientation of CTX (Figure 3E) binds to the membrane surface in an edgewise manner by involving the tips of three hydrophobic loops.

Energy Map Calculation. To see how the headgroup potential of phospholipid membranes might affect its interaction with the amphiphilic polypeptides of CTX, we adopted a mean field approach by adopting potential energy profiles previously obtained by the molecular dynamics simulation method as shown in Figure 5A. When the potential profile of the zwitterionic lipid is included to estimate the interaction energy of CTX on the DMPC membrane surface, one of the local minima can be seen to be located at the same orientation as previously determined by the FTIR method (see the upper panel of Figure 5B). Interestingly, when the potential energy profile of the negatively charged lipid is used for simulation (bottom panel of Figure 5B), similar local minimum centered

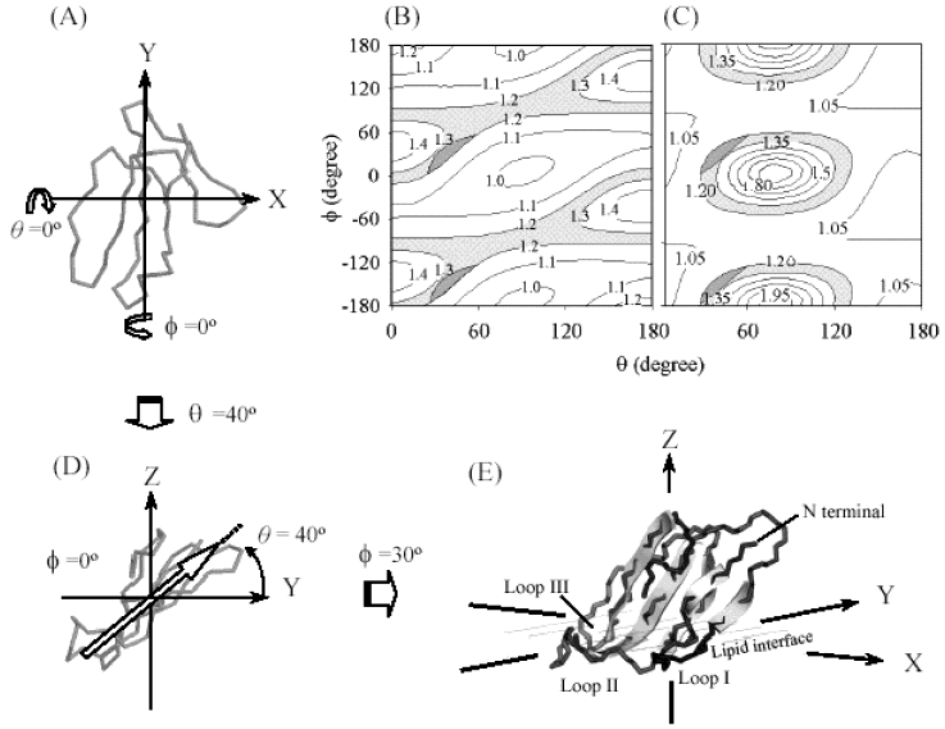

FIGURE 4: Theoretical contour plot of infrared dichroic ratio of amide I and II at designated rotation angle of CTX molecule. The original coordinate for (*q*,*f*) angle at (0,0) is arbitrarily defined for CTX molecule laying on the *xy* interface with the centered β strand aligned at the *y* axis (A). Light shadow areas represent the theoretically determined infrared dichroic ratio for those rotation angles of the CTX molecule falling within the experimentally determined values of amide I (B) or amide II (C). Dark shadow areas represent those values that are consistent with both amide I and II. Final orientation of CTX on the *xy* plane (bottom figure) can be generated by rotating the CTX molecule, initially located at the *xy* surface with the C- and N-terminals facing the *z* axis, by 40° at *the x* axis (D), followed by a 30° rotation at the *y* axis (E).

around (40°, 30°) remains. These observations further indicate that the edgewise peripheral binding mode of the CTX molecule is indeed an energy favorable state in both neutral and anionic membrane surfaces.

In addition to the edgewise binding mode in both neutral and anionic membrane surfaces, there are other energetic minima for both DMPC and DMPG membranes. For instance, the CTX A3 orientation of (90°, 30°) is also allowed in DMPC membranes according to the interaction energy consideration; however, it is not detectable by the FTIR method. While the ϕ angles of the two orientations are about the same, their θ angles deviate significantly. Qualitatively speaking, the β-sheet plane of the CTX molecule with (90°, 30°) orientation appears to be more perpendicular to the membrane surface than that with (40°, 30°) orientation. This orientation of CTX has previously been reported based on Monte Carlo simulation on P-type cardiotoxins (*42*). It is likely that, under a dehydrated condition of the sample in the ATR-FTIR experiment, CTX A3 may adopt an orientation with the lowest energy state only.

A more interesting situation can be observed for CTX on the DMPG membrane surface. Not only does the peripheral binding mode with the more perpendicular orientation of CTX A3 molecule disappear, but also an additional binding state with an inserted mode can be detected at (−10°, 50°) as depicted in the bottom panel of Figure 5B. The absence of two orientations in the peripheral binding mode of CTX A3 in the anionic membrane surface suggests a role in electrostatic interaction by preventing the fluctuation of the molecule between the two energetically allowed states of the CTX A3 molecule in the neutral membrane surface. This observation is interesting because a smaller penetration area is expected if the orientation of the CTX A3 molecule adopts a more perpendicular mode (Figure 6). Since a smaller penetration area for the peripheral binding mode adopting a more perpendicular orientation is also consistent with the so-called nonpenetrating mode identified recently by using P-type CTX from *Naja oxiano* (i.e., CT II), it would be interesting to see whether the three potential binding modes as revealed by this computer simulation study are indeed the same as those three distinct modes of CT II interaction with membranes (*43*).

CTX A3 molecules have been observed to induce leakage of vesicle contents only on negatively charged membrane surfaces (Figure 1). Therefore, the presence of the insertion mode of the CTX A3 molecule on the negatively charged membrane surface also provides a simple explanation for the observation. To verify such a possibility, we simulated the effect of a headgroup potential on the interaction energy for the presumed peripheral and insertion mode of the CTX molecule (Figure 7). Apparently, the magnitude of the membrane headgroup potential can be an efficient mechanism to modulate the distribution of CTX A3 molecules in either the peripheral or the insertion binding mode. For instance, the interaction energy becomes lower for the insertion mode rather than the peripheral binding mode when the membrane potential becomes less than 35 mV (Figure 7, inset). Such a difference in interaction energy can therefore promote the insertion mode formation as required by the leakage of vesicle contents.

Intermolecular Transfer NOE Study. Despite the similar orientation of CTX A3 against the DMPC and DMPG

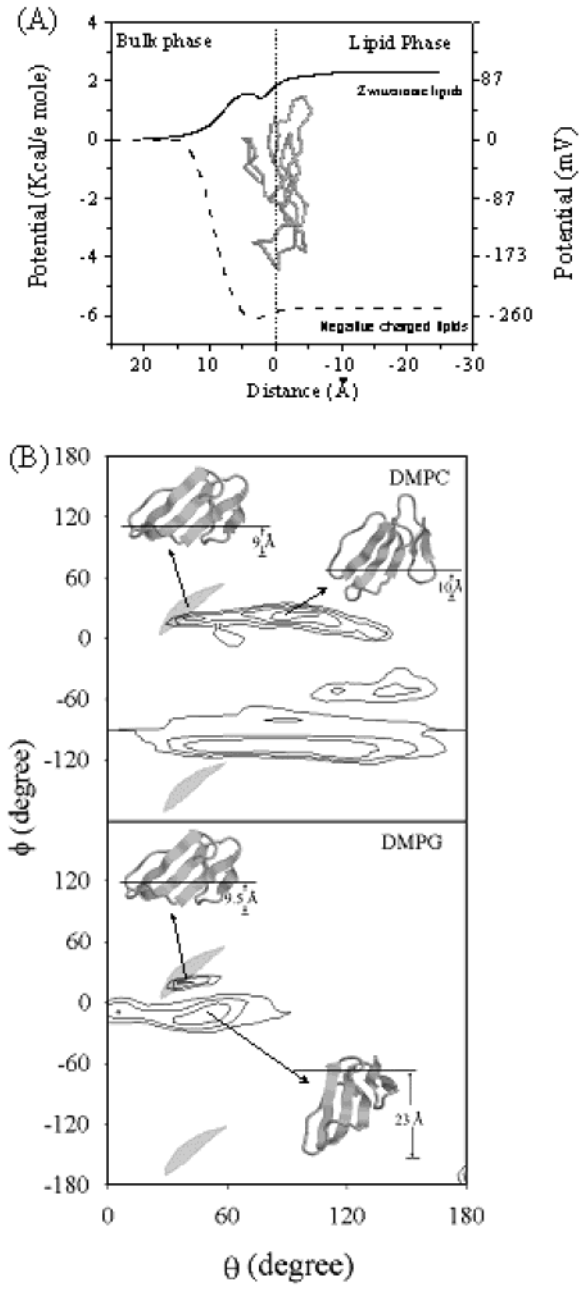

FIGURE 5: Mean field potential profile simulation to determine the optimal orientation of the CTX molecule against phospholipids monolayer. (A) Assumed mean field electrostatic potential profile of the lipid monolayer near the headgroup region as a function of penetration depth. The interface between aqueous and lipid phases is chosen to be at $z = 0$. Solid and dashed lines represent the potential profile of zwitterionic PC and negatively charged PG phospholipids at an indicated distance from the interface. (B) Equipotential contour plot of CTX/monolayer interaction energy for PC (upper panel) and PG (lower panel) monolayers by considering both the hydrophobic interaction energy and the electrostatic potential energy near the headgroup region.The energy interval of the contour plot shown in the figure is 1 kcal/mol. Shadow areas are the allowed orientation of the CTX molecule as determined by the spectroscopic method using the theoretical and experimental dichroic ratios of both amide I and II of the CTX molecule.

monolayer surface under dehydrated conditions as determined by the FTIR method, it is not known whether CTX A3 might adopt a more perpendicular form in a zwitterionic membrane surface under a fully hydrated condition as also allowed by interaction energy considerations. Such an

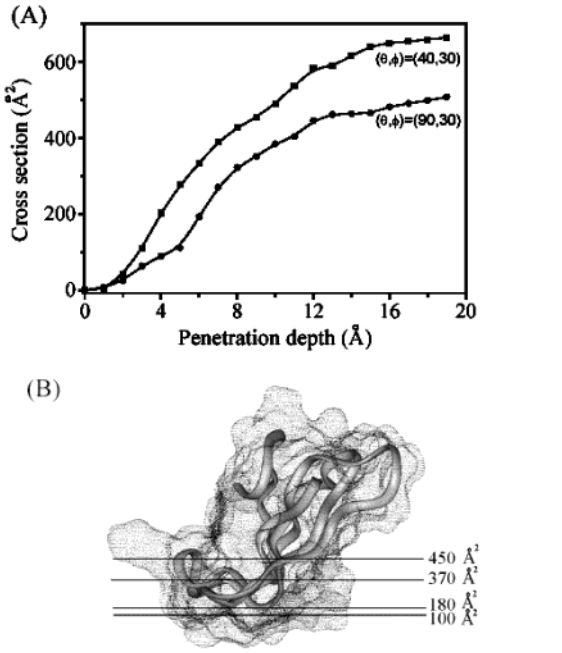

FIGURE 6: (A) Schematic diagram to show the relationship between the surface area expansion of the phospholipid monolayer and the penetration depth of the CTX molecule. (B) Ribbon and surface representation of the 3-D structure of the CTX orientation with (θ, ϕ) angles of (40°, 30°).

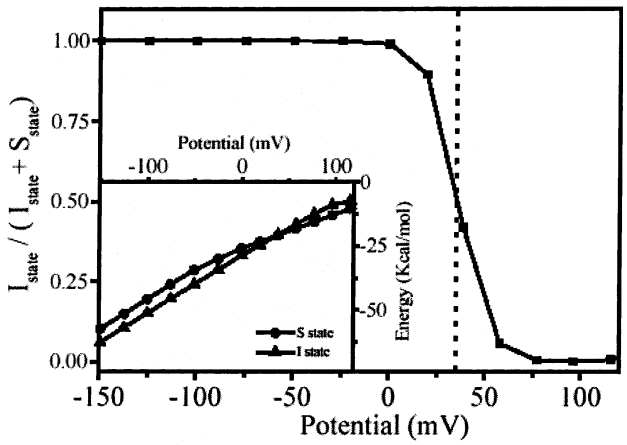

FIGURE 7: Effect of membrane potential on the inserted mode (I state) and peripheral binding mode (S state) distribution. The inserted panel shows the change of the interaction energy for both I and S states under the influence of membrane surface potential.

orientation would allow a smaller surface area expansion as shown in Figure 6A, which is based on the geometrical method. A more perpendicular orientation of the CTX molecule on the DMPC monolayer would indicate a lesser contact for the amino acid side chain located in the convex side of the CTX molecule with the fatty acyl chain of the membrane lipid. It is therefore desirable to have an independent method to monitor the penetration depth of CTX A3 into the membrane surface. One possible approach is to perform a transfer NOE NMR study on CTX/LPC micelles.

As shown in Figure 8, intermolecular transfer NOE signals can indeed be detected from the fatty acyl chain (Figure 8A) and choline methyl headgroup (Figure 8B) of LPC. It can be noted that the detectable transfer NOE signals are all located in the convex side of CTX A3 molecules, consistent with the tilting angle of the β-sheet plane of the CTX A3

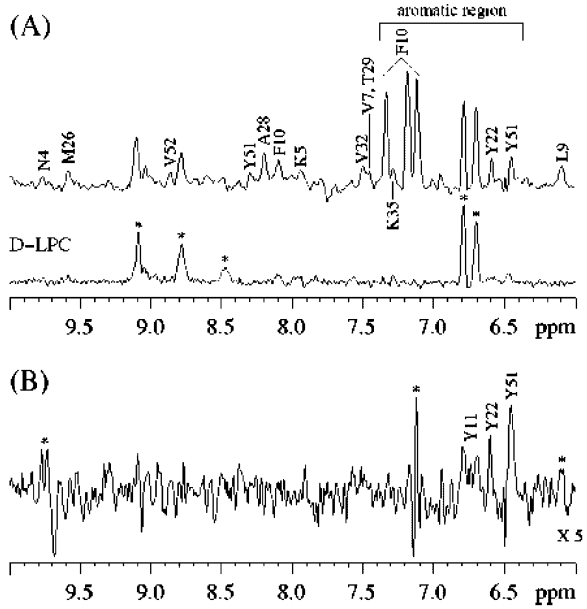

FIGURE 8: Representative 1-D NMR slices of 2-D NOESY spectra to identify the intermolecular NOEs between lysophosphatidylcholine (LPC) micelles and CTX molecules: 1-D slice at (A) 1.2 ppm for methylene, $(CH_2)_{12}$, resonance of fatty acyl chain and (B) 3.23 ppm for choline methyl, $N^+(CH_3)_3$, resonance of headgroup. Also shown in the lower trace of Figure 8A is the 1-D intermolecular NOE between the fatty acyl chain perdeuterated LPC and CTX molecules. Signals designated with * symbol are assigned as intramolecular NOEs within CTX A3. The mixing time of 150 ms and CTX/LPC ratio of 1:50 were used in this study.

molecule. For instance, all NMR signals identified to exhibit an intermolecular NOE effect with the choline methyl headgroup (i.e., Tyr11, Tyr22, and Tyr51) are located within a narrow region of the CTX A3 molecule (Figure 9). Without tilting the CTX A3 molecule toward the membrane surface, these amino acid side chains would not be close enough to allow the detection of an intermolecular NOE between the lipid headgroup and the CTX amino acid side chains. It should be emphasized that the transfer NOE effect can be detected as long as the contact time is longer than the NMR time scale (i.e., ~0.5 ns). The result does not exclude the possibility that CTX A3 might still undergo a fluctuation motion (and/or wobbling) between the two peripheral binding modes near the zwitterionic membrane surface. Nevertheless, since the NMR is performed under aqueous condition, in sharp contrast to the dehydrtated condition used for the FTIR study, it further strengthens the biochemical relevance of the conclusion made based on the FTIR and computer simulation studies.

Summary. A well-oriented sample of the CTX A3 molecule was prepared in both neutral lipid and anionic lipid monolayers transferred on a germanium ATR-plate suitable for FTIR measurement. By taking advantage of the availability of the 3-D structure of CTXs, it was demonstrated that a simple FTIR measurement on the dichroic ratio *R* of the CTX molecule yielded useful information regarding its membrane orientation. A similar approach may be useful for the determination of the orientation of amphiphilic polypeptides near the membrane surface as long as there is no dramatic conformational change within the polypeptide backbonds.

Comparative study of the peripheral binding mode of CTX A3 toward neutral and anionic membrane surface was also carried out to understand the significant difference in their respective penetration area per CTX A3 molecule. This effect is interpreted, at least partially, as a result of the electrostatic interaction between the anionic membrane surface and the cationic protein molecule to prevent the fluctuation motion of the CTX A3 molecule near the neutral membrane surface. In addition, CTX A3 appears to penetrate deeper into the negatively charged membrane surface since its peripheral binding mode is similar to that of the neutral membrane surface.

Finally, membrane headgroup potential was shown to be an efficient mechanism to account for the transition between the peripheral binding and the insertion mode. This is only possible for CTX A3 binding to the anionic membrane surface because of the presence of an additional energetic minimum to account for the insertion mode formation in the interaction energy map of CTX A3 near the anionic membrane surface. Since the anionic lipid was also shown to play a structural role in promoting the oligomerization of CTX molecules (*7*), the detected CTX A3 induced leakage of membrane vesicles in the anionic membrane surface can then be understood as a result of the oligomerization of the inserted CTX A3 molecules within the anionic phopholipid bilayers.

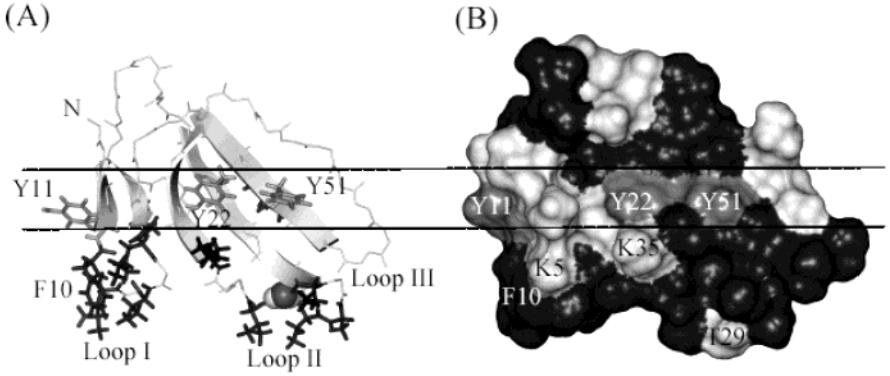

FIGURE 9: Locations of CTX amino acid residues exhibiting intermolecular NOEs with fatty acyl chain and/or choline methyls of LPC. While most of the hydrophobic residues located near the tips of the three fingered loops in the convex side were found to exhibit intermolecular NOEs with the fatty acyl group, only Tyr11, Tyr 22, and Tyr51 flanking the hydrophobic region show the intermolecular NOE with the choline methyl group. The hydrophobic residues, three Tyr residues, and hydrophilic residues were shown by black, gray, and white using a skeletal (A) and PKC (B) model of a 3-D CTX structure determined by the NMR method.

REFERENCES

1. Harvey, A. L. (1991) *Snake Toxins*, pp 259−298, Pergamon, New York.
2. Zusman, N., Miklas, T. M., Graves, T., Dambach, G. E., and Hudson, R. A. (1984) *Biochem. Biophys. Res. Commun. 124*, 629−636.
3. Zaheer, A., and Braganca, B. M. (1980) *Cancer Biochem. Biophys. 5*, 41−46.
4. Tzeng, W. F., and Chen, Y. H. (1988) *Biochem. J. 256*, 89−95.
5. Chien, K. Y., Huang, W. N., Jean, J. H., and Wu, W. (1991) *J. Biol. Chem. 266*, 3252−3259.
6. Batenburg, A. M., Bougis, P. E., Rochat, H., Verkleij, A. J., and de Kruijff, B. (1985) *Biochemistry 24*, 7101−7110.
7. Forouhar, F., Huang, W. N., Liu, J. H., Chien, K. Y., Wu, W., and Hsiao, C. D. (2003) *J. Biol. Chem.*, in press.
8. Stevens-Truss, R., and Hinman, C. L. (1997) *Toxicon 35*, 659−669.
9. Dauplais, M., Neumann, J. M., Pinkasfeld, S., Menez, A., and Roumestand, C. (1995) *Eur. J. Biochem. 230*, 213−220.
10. Dubovskii, P. V., Dementieva, D. V., Bocharov, E. V., Utkin, Y. N., and Arseniev, A. S. (2001) *J. Mol. Biol. 305*, 137−149.
11. Sue, S. C., Jarrell, H. C., Brisson, J. R., and Wu, W. (2001) *Biochemistry 40*, 12782−12794.
12. Shai, Y. (1999) *Biochim. Biophys. Acta 1462*, 55−70.
13. Huang, H. W. (2000) *Biochemistry* 39, 8347−8352.
14. Blondelle, S. E., Lohner, K., and Aguilar, M. I. (1999) *Biochim. Biophys. Acta 1462*, 89−108.
15. Heller, W. T., Waring, A. J., Lehrer, R. I., and Huang, H. W. (1998) *Biochemistry 37*, 17331−17338.
16. Sharpe, J. C., and London, E. (1999) *J. Membr. Biol. 171*, 209−221.
17. Surewicz, W. K., Stepanik, T. M., Szabo, A. G., and Mantsch, H. H. (1988) *J. Biol. Chem. 263*, 786−790.
18. Chien, K. Y., Chiang, C. M., Hseu, Y. C., Vyas, A. A., Rule, G. S., and Wu, W. (1994) *J. Biol. Chem. 269*, 14473−14483.
19. Desormeaux, A., Laroche, G., Bougis, P. E., and Pezolet, M. (1992) *Biochemistry 31*, 12173−12182.
20. Sue, S. C., Rajan, P. K., Chen, T. S., Hsieh, C. H., and Wu, W. (1997) *Biochemistry 36*, 9826−9836.
21. Lanzetta, P. A., Alvarez, L. J., and Reinach, P. S. (1979) *Anal. Biochem. 100*, 95−97.
22. Maget-Dana, R., and Ptak, M. (1997) *Biophys. J. 73*, 2527−2533.
23. Seelig, A., Blatter, X. L., Frentzel, A., and Isenberg, G. (2000) *J. Biol. Chem. 275*, 17954−17961.
24. Goormaghtigh, E., Cabiaux, J. M., and Ruysschaert, J. M. (1990) *Eur. J. Biochem. 193*, 409−420
25. Marsh, D. (1999) *Biophys. J. 77*, 2630−2637.
26. Miyazawa, T. (1960) *J. Chem. Phys. 32*, 1647−1652.
27. Marsh, D. (1997) *Biophys. J. 72*, 2710−2713.
28. Harrick, N. J. (1967) *Internal Reflection Spectroscopy*, Wiley, New York.
29. Bechor, D., and Ben-Tal, N. (2001) *Biophys. J. 80*, 643−655.
30. Milik, M., and Skolnick, J. (1993) *Proteins 15*, 10−25.
31. Biggin, P. C., and Sansom, M. S. P. (1996) *Biophys. Chem. 60*, 99−110.
32. Roseman, M. A. (1988) *J. Mol. Biol. 200*, 513−522.
33. Shnoda, W., Shmizu, M., and Okazaki, S. (1998) *J. Phys. Chem. 102*, 6647−6654.
34. Cascales, J. J. L., and Torre, J. G. (1997) *Biochim. Biophys. Acta 1330*, 145−156.
35. Rocca, P. L., Shai, Y., and Sansom, M. S. P. (1999) *Biophys. Chem. 76*, 145−159.
36. Sue, S. C., Chien, K. Y., Huang, W. N., Abraham, J. K., Chen, K. M., and Wu, W. (2002) *J. Biol. Chem. 277*, 2666−2673.
37. Bougis, P., Rochat, H., Pieroni, G., and Verge, R. (1981) *Biochemistry 20*, 4915−4920
38. Goormaghtigh, E., Raussens, V., and Ruysschaert, J. M. (1999) *Biochim. Biophys. Acta 1422*, 105−185
39. Tamm, L. K, and Tatulian, S. A. (1997) *Q. Rev. Biophys. 30*, 365−429.
40. Okamura, E., Umemura, J., and Takenaka, T. (1985) *Biochim. Biophys. Acta 812*, 139−146.
41. Cornell, D. G., and Dluhy, R. A. (1989) *Biochemistry 28*, 2789−2797.
42. Efremov, R. G., Volynsky, P. E., Nolde, D. E., Dubovskii, P. V., and Arseniev, A. S. (2002) *Biophys J. 83*, 144−153.
43. Dubovskii, P. V., Lesovoy, D. M., Dubinnyi, M. A., Utkin, Y. N., and Arseniev, A. S. (2003) *Eur. J. Biochem. 270*, 2038−2046.

BI0344477